12-26-2018

Vibrational Analysis of a Rate-Slowing Conformational Kinetic Isotope Effect

O. Maduka Ogba
Chapman University, ogba@chapman.edu

Zichen Liu
Pomona College

Daniel J. O'Leary
Pomona College

Recommended Citation
O.M. Ogba, Z.C. Liu, D.J. O'Leary, *Tetrahedron* **2019**, *75*, 545-550. doi: 10.1016/j.tet.2018.12.051

Vibrational Analysis of a Rate-Slowing Conformational Kinetic Isotope Effect

Graphical Abstract

To create your abstract, type over the instructions in the template box below.
Fonts or abstract dimensions should not be changed or altered.

Vibrational analysis of a rate-slowing conformational kinetic isotope effect

Leave this area blank for abstract info.

O. Maduka Ogba[a], Zichen Liu[b,] and Daniel J. O'Leary[b,*]

Chemistry and Biochemistry Program, Schmid College of Science and Technology, Chapman University, One University Drive, Orange CA 92866, USA
Department of Chemistry, Pomona College, 645 North College Avenue, Claremont CA 91711, USA

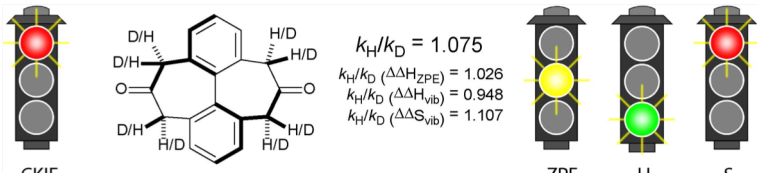

Tetrahedron
journal homepage: www.elsevier.com

Vibrational analysis of a rate-slowing conformational kinetic isotope effect

O. Maduka Ogba[a], Zichen Liu[b], and Daniel J. O'Leary[b,*]

[a] *Chemistry and Biochemistry Program, Schmid College of Science and Technology, Chapman University, One University Drive, Orange CA 92866, USA*
[b] *Department of Chemistry, Pomona College, 645 North College Avenue, Claremont CA 91711, USA*

ARTICLE INFO

Article history:
Received
Received in revised form
Accepted
Available online

Keywords:
Conformational Kinetic Isotope Effect
Ab initio calculations
Biaryls
Chirality
Conformational analysis
Isotope effects

ABSTRACT

An enthalpy-entropy approach to analyzing a rate-slowing conformational kinetic isotope effect (CKIE) in a deuterated doubly-bridged biaryl system is described. The computed isotope effect (k_H/k_D = 1.075, 368 K) agrees well with the measured value (k_H/k_D = 1.06, 368 K). The rate-slowing (normal isotope effect) nature of the computed CKIE is shown to originate from a vibrational entropy contribution defined by the twenty lowest frequency normal modes in the ground state and transition state structures. This normal entropy contribution is offset by an inverse vibrational enthalpy contribution, which also arises from the twenty lowest frequency normal modes. Zero point vibrational energy contributions are found to be relatively small when all normal modes are considered. Analysis of the H_{ZPE}, H_{vib}, and S_{vib} energy terms arising from the low frequency vibrational modes reveals their signs and magnitudes are determined by larger vibrational energy differences in the labeled and unlabeled ground state structures.

1. Introduction

The conformational kinetic isotope effect (CKIE) in biaryl diketone **1**-d_8 is a rare example of a rate-slowing CKIE.[1,2] The observed k_H/k_D =1.06 (368 K) in diketone **1** is regarded as a normal isotope effect, as many processes, bond-breaking included, are slowed by deuterium substitution. What makes the CKIE in diketone **1** somewhat unique is that the majority of CKIEs are inverse (k_H/k_D < 1). Deuterium substitution generally increases isomerization rates, especially those involving compression of C–H/D bonds. A textbook[3] example is dihydrodimethylphenanthrene **2**-d_6, whose k_H/k_D = 0.880 (315 K) was taken as evidence of a steric isotope effect.[4,5]

We have used computational methods to study CKIEs in these and related molecules and have probed the factors responsible for their opposite behavior.[6,7] These previous studies suggest CKIE predictions are reasonably accurate and independent of theoretical approach (HF, DFT, MP2, etc.) and basis sets. Our original motivation for studying diketone **1** stemmed from an intriguing suggestion that its normal isotope effect might be due to a *larger* effective size of deuterium. This proposal was based upon neutron-diffraction studies of benzene and benzene-d_6 in the solid state, where the latter exhibits a larger molar volume at elevated temperatures.[8] In our studies of **1** and **2**, we discovered their KIEs originate from enthalpic and entropic terms of vibrational origin, and these contributions are often antagonistic and are sometimes dominated by the entropy term. In diketone **1** for example, computed Bigeleisen-Mayer (B-M) terms[9] for the CKIE are: ZPE (1.026), EXC (1.050) and MMI (0.998). The computed enthalpy-entropy (*H*-*S*) contributions are $\Delta\Delta H_{ZPE}$ (1.026), $\Delta\Delta H_{vib}$ (0.948), $\Delta\Delta S_{vib}$ (1.107), and $\Delta\Delta S_{rot}$ (0.998) (Table 1).

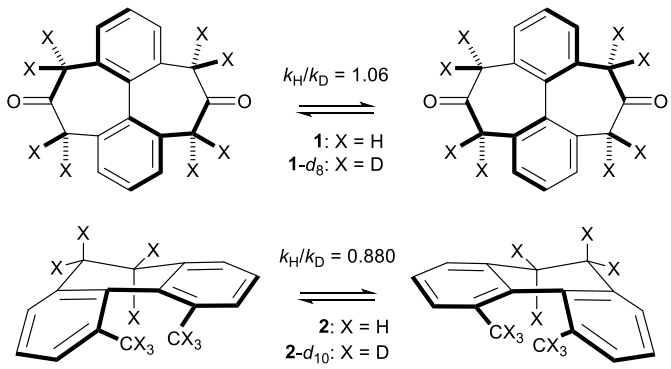

Figure 1. Kinetic isotope effects observed experimentally in the isomerization of doubly bridged biaryl diketone **1** and dihydrodimethylphenanthrene **2**.

In our view, the use of enthalpy-entropy contributions to understand isotope effects is often preferable to the more commonly used Bigeleisen-Mayer partition functions because the former can be, and have been, experimentally determined and compared with theory.[5,6] The relationship between the B-M and *H*-*S* terms is shown in Figure 2. Enthalpic zero-point vibrational

* Corresponding author. Tel.: +0-000-000-0000; fax: +0-000-000-0000; e-mail: author@university.edu

energy (ZPE) differences arising from high frequency normal modes are the cause of many isotope effects. However, it is known through computational investigations that thermal excitation of low frequency modes can affect isotope effects. These include **1** and **2** and related systems,[6,7] amide bond rotation,[10,11] metal-H_2 and metal C–H interactions,[12] and equilibrium isotope effects in intramolecular OH/OH hydrogen bonds.[13]

The purpose of this study is to provide a clearer understanding of the normal CKIE in biaryl diketone **1**. At the conclusion of our 2012 study,[7] we projected the need to quantify, in systems like **1**, the vibrational frequency dependence of the $\Delta\Delta H_{vib}$ and $\Delta\Delta S_{vib}$ contributions to the CKIE.[7] At the time, we felt a full treatment would require a quantitative linkage of vibrational frequencies with enthalpic and entropic contributions to the isotope effect. Herein, we report the results of our investigation.

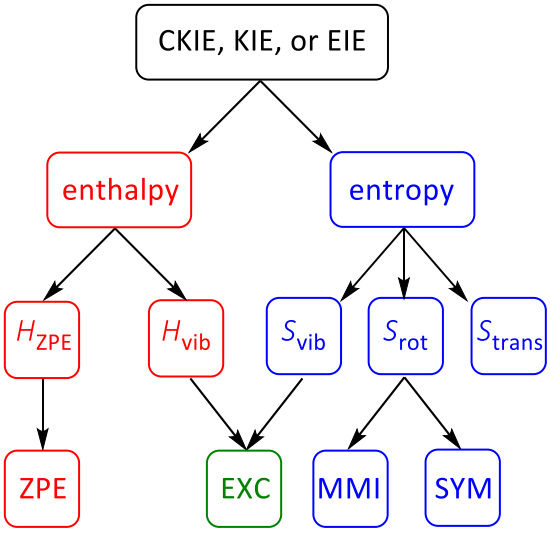

Figure 2. A flowchart showing how a CKIE, kinetic isotope effect (KIE) or equilibrium isotope effect (EIE) partitions into enthalpy and entropy contributions and their relationship to the B-M ZPE, EXC, MMI, and SYM contributions.

2. Results and Discussion

We previously reported the computed potential energy surface and conformational KIE for the racemization of **1**.[6,7] The barrier ($\Delta H^{‡}$ = 28.5 kcal/mol) and KIE (k_H/k_D = 1.075, 368 K) are consistent with experimental reports[1,2] (Figure 2). Vibrational analysis of the transition state structure revealed that the imaginary vibrational mode on the reaction trajectory is the wagging of one of the four bridging methylene CH_2 groups; the stationary structure reveals that in the transition state (**TS-1**), the two CH_2 protons are positioned staggered with respect to the adjacent carbonyl C=O, while in the ground state **1**, one of the C–H/D bonds is positioned eclipsed to the C=O (Figure 3, Bottom). Intrinsic reaction coordinate (IRC) analysis of the transition state structure revealed a high energy C_{2h} intermediate following **TS-1** on the potential energy surface. The presence of this achiral C_{2h} intermediate provides a racemization pathway in this system.

The enthalpy and entropy terms factor into the KIE expression according to Eqs. 1-12[14], using the reactant (*R*), transition state (‡) label convention and defining the universal gas constant as R_g:

$$\left(\frac{k_H}{k_D}\right)_{\Delta\Delta H} = e^{\Delta\Delta H/R_g T} \quad (1)$$

$$\Delta\Delta H = \left(H_D^{‡} - H_D^{R}\right) - \left(H_H^{‡} - H_H^{R}\right) \quad (2)$$

(or)

$$\Delta\Delta H = \left(H_D^{‡} - H_H^{‡}\right) + \left(H_H^{R} - H_D^{R}\right) \quad (3)$$

$$\left(\frac{k_H}{k_D}\right)_{\Delta\Delta S} = e^{\Delta\Delta S/R_g} \quad (4)$$

$$\Delta\Delta S = \left(S_H^{‡} - S_H^{R}\right) - \left(S_D^{‡} - S_D^{R}\right) \quad (5)$$

(or)

$$\Delta\Delta S = \left(S_H^{‡} - S_D^{‡}\right) + \left(S_D^{R} - S_H^{R}\right) \quad (6)$$

The enthalpy and entropy contributions combine as their products to determine the overall isotope effect:

$$KIE = \left(\frac{k_H}{k_D}\right)_{\Delta\Delta G} = e^{\Delta\Delta H^{‡}/R_g T} \times e^{\Delta\Delta S^{‡}/R_g} = e^{\Delta\Delta G^{‡}/R_g T} \quad (7)$$

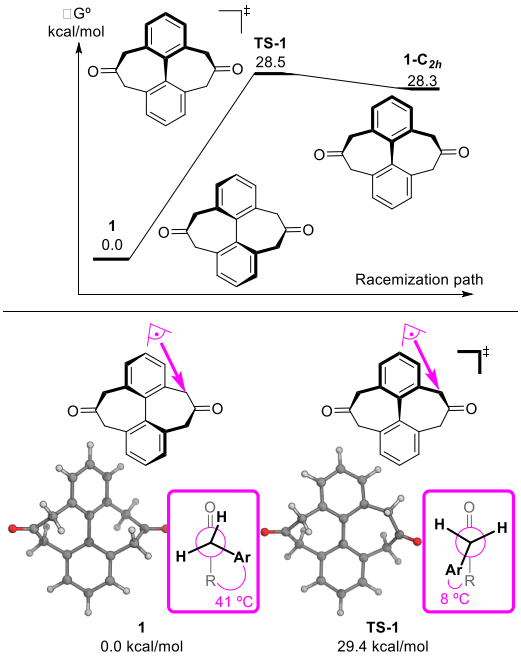

Figure 3. Computed B3LYP 6-31G(d,p) potential energy surface for racemization of **1** (Top). Minimum energy ground and transition state structure, and Newman projection of key methylene CH_2 group associated with the wagging motion in the imaginary vibrational mode in **TS-1** (Bottom).

The extracted frequencies and rotational temperatures can be used to directly compute the isotope-dependent vibrational and rotational contributions to the enthalpy and entropy.[15,16] The enthalpic internal thermal energy, defined here as $H_{thermal}$, can be written as the sum of the zero-point energy and a temperature-dependent vibrational term:

$$H_{thermal} = H_{ZPE} + H_{vib} \quad (8)$$

$$H_{ZPE} = R_g \sum \frac{\theta_v}{2} \quad (9)$$

$$H_{vib} = R_g \sum \frac{\theta_v}{e^{\theta_v/T} - 1} \quad (10)$$

where $\theta_v = h\nu/k$ is the characteristic vibrational temperature.

Entropy has vibrational and rotational terms dependent upon isotopic substitution (Eq. 11). Only the vibrational term is presented here, as the rotational term does not make significant contributions to the CKIE in these systems (Table 1).

$$S = S_{vib} + S_{rot} \quad (11)$$

$$S_{vib} = R_g \sum \left(\frac{\theta_v/T}{e^{\theta_v/T} - 1} - \ln\left(1 - e^{-\theta_v/T}\right) \right) \quad (12)$$

The vibrational entropy contribution (Eq. 12) is a function of the temperature and the aforementioned characteristic vibrational temperatures.

The contributions of enthalpy and entropy terms, and the corresponding Bigeleisen-Mayer terms, are compiled for four sets of frequency ranges in Table 1. The frequency ranges are defined by low (modes 1-20, 0-500 cm^{-1}), medium (modes 21-82, 500-1720 cm^{-1}), high (modes 83-96, 2100-3100 cm^{-1}), and all frequencies (modes 1-96). The table entries are color coded, with yellow cells identifying KIE contributions of less than ±3% (defined here as small contributions), red identifying contributions greater than 5% slowing racemization (normal isotope effect), and green identifying contributions greater than 5% speeding racemization (inverse isotope effect).

Based upon our earlier work, several familiar trends in the frequency-binned data are evident: 1. The high frequency C–H/D stretching terms do not appreciably contribute to the isotope effect (k_H/k_D = 1.019, modes 83-96), and 2. While the B-M EXC term is reasonably large (k_H/k_D = 1.050, modes 1-96) and defined primarily by low frequency modes 1-20, the *H-S* dissection shows this term is a composite of antagonistic $\Delta\Delta H_{vib}$ (k_H/k_D = 0.948, modes 1-96) and $\Delta\Delta S_{vib}$ (k_H/k_D = 1.107, modes 1-96) terms. The dominant $\Delta\Delta S_{vib}$ term can be thought of as determining the normal nature of the overall CKIE. However, a different observation arose from the new analysis: the $\Delta\Delta H_{ZPE}$ term is small (k_H/k_D = 1.026, modes 1-96) when all frequencies are taken into consideration, but interestingly, this arises as a consequence of antagonistic low (k_H/k_D = 1.123, modes 1-20) and medium frequency-derived (k_H/k_D = 0.896, modes 21-82) terms (Table 1).

Table 1. Bigeleisen-Mayer (B-M) and enthalpy-entropy (*H-S*) term contributions to the overall KIE (k_H/k_D) in biaryl diketone **1** using low, mid, and high vibrational frequency ranges. Yellow cells: KIE contributions less than 3%. Red cells: normal KIE contributions greater than 5%, slowing racemization. Green cells: inverse KIE contributions greater than 5%, speeding racemization.

k_H/k_D term	Low frequencies Modes 1-20[a]	Mid Frequencies Modes 21-82[b]	High Frequencies Modes 83-96[c]	All Frequencies Modes 1-96
	Bigeleisen-Mayer Analysis			
ZPE	1.123	0.896	1.020	1.026
EXC	1.052	0.998	1.000	1.050
MMI	0.998	0.998	0.998	0.998
B-M (overall)	1.179	0.892	1.019	1.075
	Enthalpy-Entropy Analysis			
$\Delta\Delta H_{ZPE}$	1.123	0.896	1.020	1.026
$\Delta\Delta H_{vib}$	0.943	1.005	1.000	0.948
$\Delta\Delta S_{vib}$	1.116	0.992	1.000	1.107
$\Delta\Delta S_{rot}$	0.998	0.998	0.998	0.998
H-S (overall)	1.179	0.892	1.019	1.075

[a]0-500 cm^{-1}. [b]500-1780 cm^{-1}. [c]2100-3100 cm^{-1}.

We next explored the contributions of individual normal modes to $\Delta\Delta H_{ZPE}$, $\Delta\Delta H_{vib}$, and $\Delta\Delta S_{vib}$, respectively. There are 96 vibrational modes in ground state **1** and 95 in transition state **TS-1**. We set out to unravel the energetic contribution of each vibrational mode on the KIE associated with the $\Delta\Delta H_{ZPE}$, $\Delta\Delta H_{vib}$, and $\Delta\Delta S_{vib}$ *H-S* terms. The plots in Figure 4 depict the vibrational mode-dependent values of H_{ZPE}, H_{vib}, and S_{vib}, computed using Eqs. 9, 10, and 12, respectively, for the labeled and unlabeled ground state and transition state structures.

As expected from the form of Eq. 9, H_{ZPE} increases across the range of low to medium frequencies (0 -1780 cm^{-1}) and spans energies ranging 0-4.45 kcal/mol. The H_{ZPE} contributions for the

low frequency vibrations (modes 1-20) of the unlabeled and labeled forms of GS-**1** and TS-**1** *appear* to be largely equivalent, an interpretation at odds with the large normal CKIE contribution for these modes (k_H/k_D ($\Delta\Delta H_{ZPE}$) = 1.123). The H_{ZPE} energies for modes 21-82 skew to lower values for contributions across the medium frequencies, as one might expect for the mass-dependent vibrational frequencies, and this trend gives rise to the large inverse CKIE contribution for these modes (k_H/k_D ($\Delta\Delta H_{ZPE}$) = 0.896). The high frequency C–H/D stretching terms (2100-3100 cm^{-1}), are expected to have large differences for an isolated C–D or C–H stretch, but the overall summation of these terms for modes 83-96 (Eqs. 2 or 3) produces only a 2% contribution to the CKIE (k_H/k_D ($\Delta\Delta H_{ZPE}$) = 1.020).

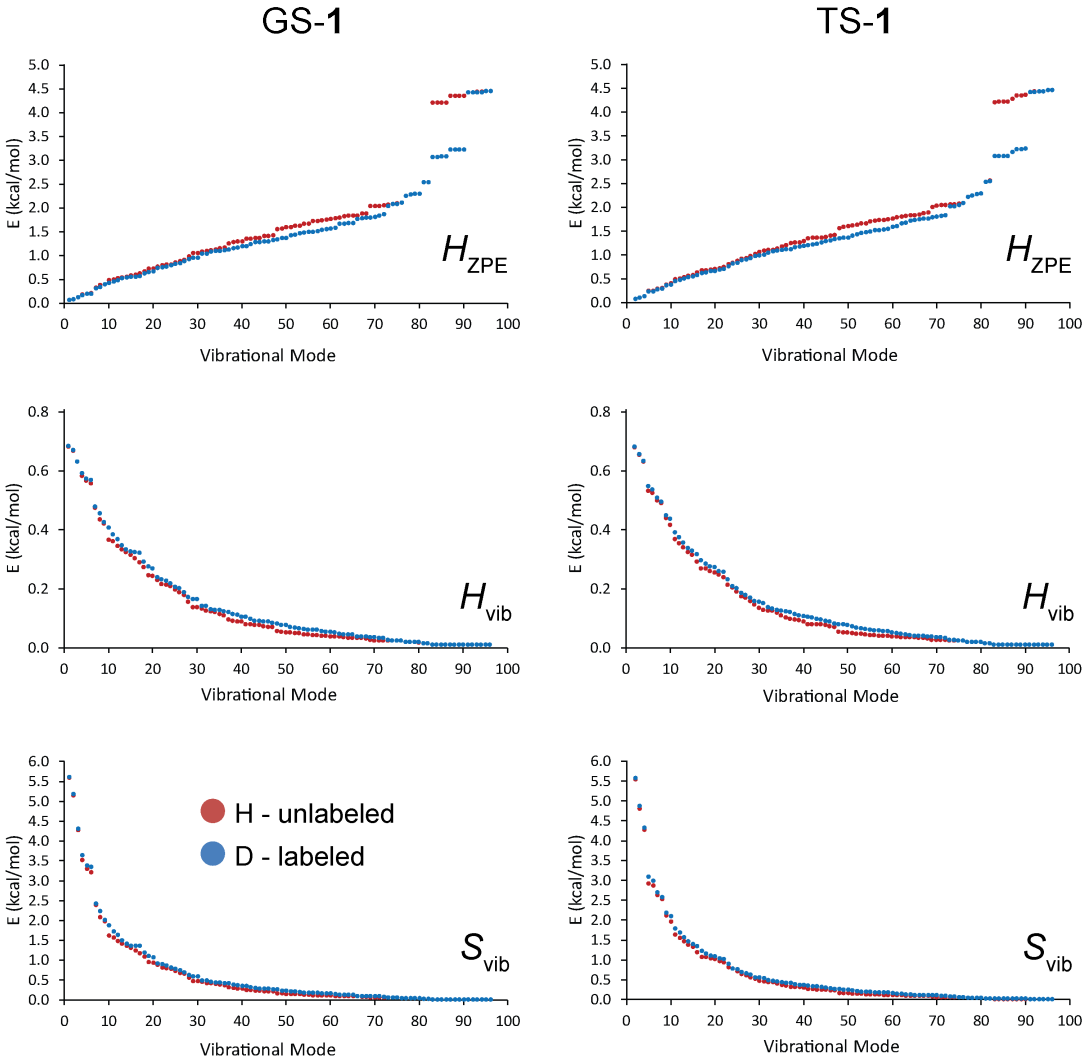

Figure 4. Plots of H_{ZPE}, H_{vib}, and S_{vib} (kcal/mol) as a function of vibrational mode in unlabeled and labeled ground state (**GS-1**) and transition state structures (**TS-1**). Modes 1-20 = 0-500 cm^{-1}, modes 21-82 = 500-1780 cm^{-1}, modes 83-96 = 2100-3100 cm^{-1}.

While the functional forms of H_{vib} (Eq. 10) and S_{vib} (Eq. 12) are different, each of their plots in Figure 4 show exponential decreases in energy with increasing vibrational frequency. It is interesting to note that the H_{vib} and S_{vib} energies arising from the labeled species trend to larger values than those from unlabeled structures. This is opposite to what is observed for the H_{ZPE} curves and is a consequence of the form of the respective equations. It also provides a graphical representation of the thermal excitability of the lower frequencies associated with heavy atom substitution. The degree of curvature is more pronounced for S_{vib}, whose energies span a range from 0-5.6 kcal/mol, similar to those for H_{ZPE}. The energy range for H_{vib} (0-0.67 kcal/mol) is approximately eight times smaller than that of H_{ZPE} or S_{vib}. The mode-specific contributions of H_{vib} and S_{vib} to the CKIE arise from the lowest vibrational frequencies. As seen in Table 1, modes 1-20 produce antagonistic contributions, with k_H/k_D ($\Delta\Delta H_{vib}$) = 0.943 and k_H/k_D ($\Delta\Delta S_{vib}$) = 1.116.

We next studied the possibility of mapping the mode-specific H_{ZPE}, H_{vib}, and S_{vib} terms onto the normal modes of the unlabeled and labeled GS and TS structures. Our goal was to correlate a ΔH_{vib} term with an unlabeled and labeled GS normal mode, so that we could identify those modes that make the largest contribution to the CKIE. This proposition, while workable for a CKIE determined by a small number of vibrational modes, such as the

steric compression of a single C–H/D bond,[7,17,18] proved impossible for biaryl diketone **1**. The intractable part of the problem are the medium-range vibrational frequencies (modes 21-82, 500-1780 cm^{-1}). Across this range, the normal modes for an unlabeled and labeled GS (or TS) structure become highly mixed and unique in terms of their atomic motions. On the other hand, a root mean square difference (RMSD) analysis of normal mode atom displacements showed that it is possible to match the modes of unlabeled and labeled GS and TS structures for the lowest (modes 1-20) and the highest (modes 83-96) frequencies. It is important to note that we are not saying that any of these mode pairs for an unlabeled/labeled species are precisely identical. But a viewer of the animated normal modes would conclude that the mode pairs are highly similar, and we thus are able to compute estimates of mode-specific energy contributions.

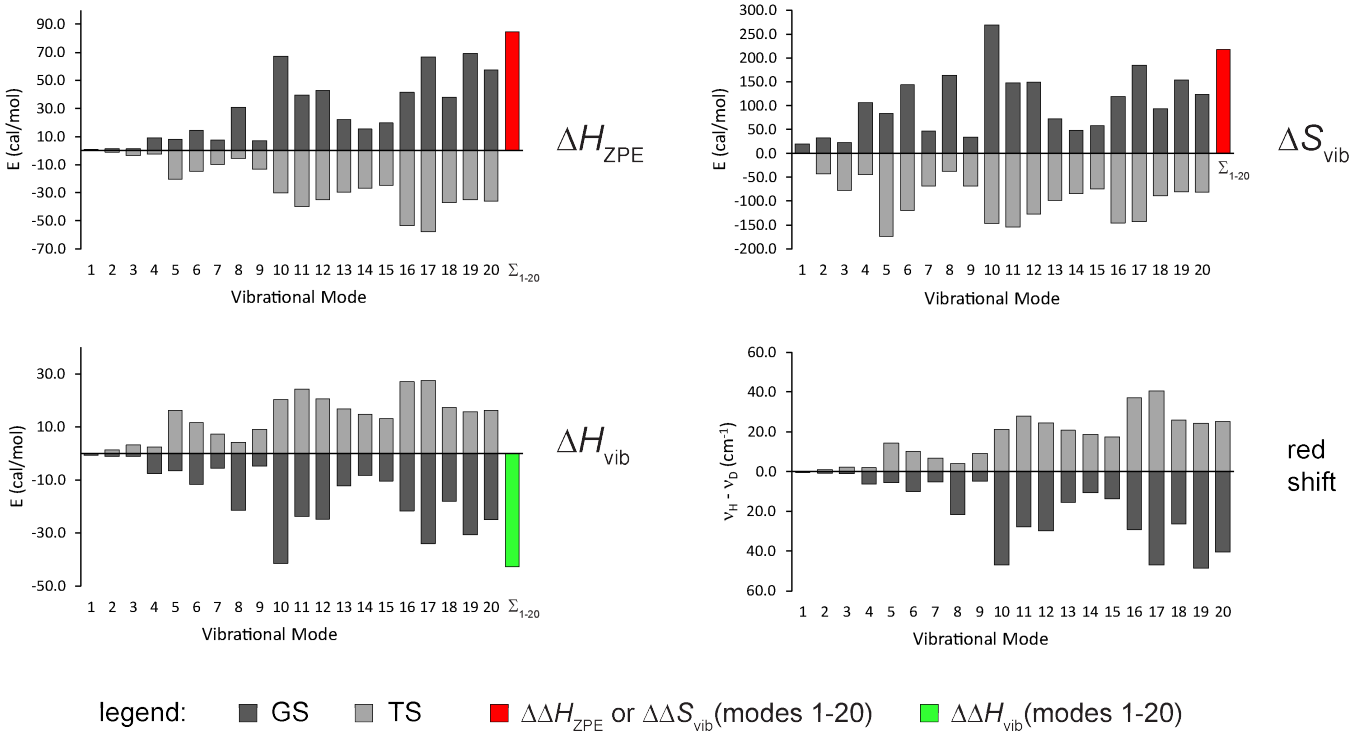

Figure 5. Plots of ΔH_{ZPE}, ΔH_{vib}, and ΔS_{vib} (cal/mol) as a function of vibrational mode in unlabeled and labeled ground state (**GS-1**, charcoal) and transition state structures (**TS-1**, grey) for modes 1-20 (0-500 cm^{-1}) using Eqs. 3 and 6. The summation terms $\Delta\Delta H_{ZPE}$, $\Delta\Delta H_{vib}$, and $\Delta\Delta S_{vib}$ over these modes are coded red for racemization-slowing and green for racemization-speeding. Lower right: Plot of red shift (ν_H - ν_D, cm^{-1}) for modes 1-20 in unlabeled and labeled **GS-1** and **TS-1** structures.

Having identified matched low frequency modes within GS and TS structures, we then plotted the ΔH_{ZPE}, ΔH_{vib}, and ΔS_{vib} terms using Eqs. 3 and 6 for each GS or TS mode (Figure 5). When presented in this manner, certain GS and TS vibrational modes can be identified as large (GS mode 10) or small (GS mode 9) contributors. These differences can be largely attributed to the red shift caused by isotopic substitution. For GS mode 9, the shift is 5.2 cm^{-1} and for GS mode 10 it is 48.5 cm^{-1}. The former mode is a symmetric breathing mode, whereas the latter is a CH_2/CD_2 wagging mode. A plot of the red shifted frequency differences (Figure 5) reveals a correlation between the magnitude of the frequency differences and the energy terms on the adjacent plots. However, these correlations are straightforward only in the case of H_{ZPE}, whose functional form is linear. It is also evident that the signs and magnitudes of the summative terms $\Delta\Delta H_{ZPE}$, $\Delta\Delta H_{vib}$, and $\Delta\Delta S_{vib}$ are each determined by larger energy differences arising from modes associated with the ground state (Figure 5). It is also important to emphasize that the mode-specific GS and TS energy terms bear no meaningful relationship to each other, as the atomic motions in each are fundamentally unique.

3. Conclusion

The conformational kinetic isotope effects for the racemization of biaryl diketone **1** and **1**-d_8 was probed via a detailed analysis of computed harmonic vibrational frequencies. The normal (KIE = 1.075) is most significantly due to a dominant vibrational entropy contribution, although this is scaled by an antagonistic vibrational enthalpy contribution (H_{vib}) that is not related to zero point vibrational differences (H_{ZPE}). Across all vibrational modes, H_{ZPE} contributes the least to the CKIE when compared with H_{vib} and S_{vib}. However, the H_{ZPE} term exhibits frequency-dependent antagonistic behavior and provides a large normal contribution from low frequency modes, a large inverse contribution from medium frequency modes, and a small normal contribution from high frequency modes. Analysis of the summative effect of low frequency vibrational modes for H_{ZPE}, H_{vib}, and S_{vib} reveals that the sign and magnitude of these energy terms are determined by larger vibrational energy differences in the labeled and unlabeled ground state structures.

The protocol described in this work is currently being used to investigate other racemizations/isomerizations in an effort to test the generality of the observations reported here.

4. Experimental Section

The methodology for computing vibrational frequencies was based upon similar work in the literature. Quantum mechanical calculations of harmonic vibrational frequencies and thermochemistry were performed in the gas phase at the B3LYP[19]/6-31G(d,p)[20,21] level of theory using Gaussian 09.[22] All vibrational frequencies were scaled at 0.97. Isotope effects were calculated with a spreadsheet[14] or with *Onyx*.[23]

5. Acknowledgments

The authors thank Pomona College for funding this study, and we thank Asya Shklyar (Pomona College High Performance Computing Facility) for her assistance. O.M.O. thanks Pomona College for provision of a Robbins Post-Doctoral fellowship.

6. Supplementary Material

Optimized geometries, energies, unscaled frequencies, intrinsic reaction coordinate (IRC) path, and H_{ZPE}, H_{vib}, and S_{vib} contributions for all normal modes in GS-**1** and TS-**1**.

References and Notes

1. Mislow, K.; Simon, E.; Hopps, H. B. *Tetrahedron Letters* **1962**, 1011-1014.
2. Mislow, K.; Simon, E.; Glass, M. A. W.; Wahl, G. H.; Hopps, H. B. *Journal of the American Chemical Society* **1964,** *86*, 1710-1733.
3. Anslyn, E. V.; Dougherty, D. A. *Modern physical organic chemistry*; University Science: Sausalito, CA, 2006.
4. Mislow, K. G., R.; Gordon, A.J.; Wahl, G.H. *Journal of the American Chemical Society* **1963,** *85*, 1199-1200.
5. Mislow, K.; Wahl, G. H.; Gordon, A. J.; Graeve, R. *Journal of the American Chemical Society* **1964,** *86*, 1733-1741.
6. O'Leary, D. J.; Rablen, P. R.; Meyer, M. P. *Angewandte Chemie-International Edition* **2011,** *50*, 2564-2567.
7. Fong, A.; Meyer, M. P.; O'Leary, D. J. *Molecules* **2013,** *18*, 2281-2296.
8. Dunitz, J. D.; Ibberson, R. M. *Angewandte Chemie-International Edition* **2008,** *47*, 4208-4210.
9. Bigeleisen, J.; Mayer, M. G. *Journal of Chemical Physics* **1947,** *15*, 261-267.
10. Perrin, C. L.; Thoburn, J. D.; Kresge, A. J. *Journal of the American Chemical Society* **1992,** *114*, 8800-8807.
11. Olson, L. P.; Li, Y.; Houk, K. N.; Kresge, A. J.; Schaad, L. J. *Journal of the American Chemical Society* **1995,** *117*, 2992-2997.
12. Parkin, G. *Journal of Labelled Compounds & Radiopharmaceuticals* **2007,** *50*, 1088-1114.
13. O'Leary, D. J.; Hickstein, D. D.; Hansen, B. K.; Hansen, P. E. *Journal of Organic Chemistry* **2010,** *75*, 1331-42.
14. Ogba, O. M.; Thoburn, J. D.; O Leary, D. J. In *Applied theoretical organic chemistry;* Tantillo, D. J. Ed.; World Scientific: New Jersey, 2018; pp. 403-450.
15. Laurendeau, N. M. *Statistical thermodynamics: fundamentals and applications*; Cambridge University Press: New York, 2005.
16. Ochterski, J. W. Thermochemistry in Gaussian. http://gaussian.com/thermo/ (accessed October 1, 2018).
17. Sherrod, S. A.; Boekelheide, V. *Journal of the American Chemical Society* **1972,** *94*, 5513-5515.
18. Sherrod, S. A.; Costa, R. L. D.; Barnes, R. A.; Boekelheide, V. *Journal of the American Chemical Society* **1974,** *96*, 1565-1577.
19. Becke, A. D. *Journal of Chemical Physics* **1993,** *98*, 5648-5652.
20. Ditchfield, R.; Hehre, W. J.; Pople, J. A. *Journal of Chemical Physics* **1971,** *54*, 724-+.
21. Harihara.Pc; Pople, J. A. *Theoretica Chimica Acta* **1973,** *28*, 213-222.
22. Frisch, M. J.; Trucks, G. W.; Schlegel, H. B.; Scuseria, G. E.; Robb, M. A.; Cheeseman, J. R.; Scalmani, G.; Barone, V.; Petersson, G. A.; Nakatsuji, H.; Li, X.; Caricato, M.; Marenich, A.; Bloino, J.; Janesko, B. G.; Gomperts, R.; Mennucci, B.; Hratchian, H. P.; Ortiz, J. V.; Izmaylov, A. F.; Sonnenberg, J. L.; Williams-Young, D.; Ding, F.; Lipparini, F.; Egidi, F.; Goings, J.; Peng, B.; Petrone, A.; Henderson, T.; Ranasinghe, D.; Zakrewski, V. G.; Gao, J.; Rega, N.; Zheng, G.; Liang, W.; Hada, M.; Ehara, M.; Toyota, K.; Fukuda, R.; Hasegawa, J.; Ishida, M.; Nakajima, T.; Honda, Y.; Kitao, O.; Nakai, H.; Vreven, T.; Throssell, K.; Montgomery, J. A.; Peralta, J. E.; Ogliaro, F.; Bearpark, M.; Heyd, J. J.; Brothers, E.; Kudin, K. N.; Staroverov, V. N.; Keith, T.; Kobayashi, R.; Normand, J.; Raghavachari, K.; Rendell, A.; Burant, J. C.; Iyengar, S. S.; J., T.; Cossi, M.; Millam, J. M.; Klene, M.; Adamo, C.; Cammi, R.; Ochterski, J. W.; L., M. R.; Morokuma, K.; O., F.; Foresman, J. B.; Fox, D. J. *Gaussian 09, Revision C.02*, Gaussian, Inc.: Wallingford CT, 2016.
23. Brueckner, A. C.; Cevallos, S. L.; Ogba, O. M.; Walden, D. M.; Meyer, M. P.; O'Leary, D. J.; Cheong, P. H.-Y. *Onyx, version 1.0; Oregon State University: Corvallis, OR, USA & Pomona College: Claremont, CA, USA, 2016.*